Proceedings of the 2003 IEEE/RSJ
Intl. Conference on Intelligent Robots and Systems
Las Vegas, Nevada · October 2003

Force-Guided Assembly of Micro Mirrors

Yantao Shen and Ning Xi
Dept. of Electrical and Computer Engr.
Michigan State University
East Lansing, MI 48824
USA

Wen Jung Li
Dept. of Automation and Computer-Aided Engr.
The Chinese University of Hong Kong
Shatin, N. T., Hong Kong SAR
CHINA

Abstract— **This paper aims at developing the force-guided microassembly technology with in-situ PVDF piezoelectric force sensing and control. By using the designed force sensors with the effective signal processing techniques, the micro contact force/impact signal and its derivative can be extracted and processed. Furthermore, based on a new sensor-referenced control scheme, micro mirrors can be reliably assembled by regulating the micro contact force. Experimental results verify the performance of the developed micro force sensing and control system. Ultimately the technology will provide a critical and major step towards the development of automated manufacturing processes for batch assembly of micro devices.**

I. INTRODUCTION

Manufacturing processes which are capable of efficiently assembling MEMS devices such 3-D optomechanical micro mirrors in optical switches have not been developed, partially because, at the micro-scale, structures are fragile and easily breakable. They typically break at the micro-Newton force range that cannot be reliably measured by the most existing force sensors [4]. The micro mirror components usually lie on the surface of substrate after fabrication processes, as shown in Figure 1(a). An assembly process is needed to lift it up to an upright position as shown in Figure 1(b). Currently, besides non-contact batch assembly techniques developed [1], the most straightforward and flexible methods are still to use microprobe to physically manipulate the mirror into the position [2]. However, those processes can be inherently risky without knowledge of the force(s) being applied. As a result, this situation decreases overall yield and driving up cost of micro devices [3]. For these reasons, researches into automating the microassembly processes have focused on the micro force sensing and control techniques. Currently, there exist some developing sensing mechanisms commonly used in sensing contact forces in microassembly [4]. Among those mechanisms, more suitably, the resolution of force sensors based on piezoelectric effect is in the range of μN generally. Furthermore, the development of force regulation schemes is necessary because big impact and contact forces may break the micro structures such as micro mirrors during microassembly. Recently, a low level proportional impact force control scheme using nano scale optical beam deflection force feedback, has been implemented to reduce the large impact effects [5]. In [6], Tanikawa et al. present a force control system whose task is to keep a proper constant force during the grasp micromanipulation. Unfortunately, as the authors report in the paper, the high success rate of the grasp task can not be obtained with a stiffness-like-force-control scheme. It is reasonable to state that a very few successful micro contact/impact force controllers have been reported. However, it is absolutely necessary to develop a robust contact/impact force controller to achieve a reliable and efficient microassembly.

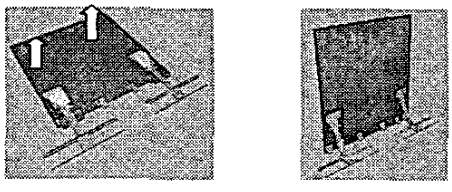

(a) (b)

Fig. 1. Micro mirror assembly: (a) a force is applied at the mirror. (b) the automatic latches lock the mirror in upright position.

The objective of this paper is to develop a feasible and versatile solution in the force-guided microassembly, i.e., designing a highly sensitive force sensor to measure micro contact/impact force and its rate, and then enables a regulation of micro contact/impact force during the microassembly, especially in the assembly of the 3-D micro mirrors. Piezoelectric material such as polyvinylidene fluoride (PVDF) is highly sensitive to deflection [7]. Upon this property of PVDF, a high sensitivity micro force and force rate sensor is developed to detect the micro contact force and its derivative signals during microassembly, and the signals can then be fed back and regulated by a new sensor-referenced force control scheme. The experiments on reliably lifting up the micro mirrors demonstrate the performances of the developed micro force control and assembly schemes. This could be an important step to make reliable and high yield batch fabrication and assembly of micro devices a reality.

II. FORCE SENSING MODEL

A. Sensor Models

As shown in Figure 2, a 1-D PVDF sensor model can be developed. Based on the piezoelectric effect, the unit

0-7803-7860-1/03/$17.00 © 2003 IEEE

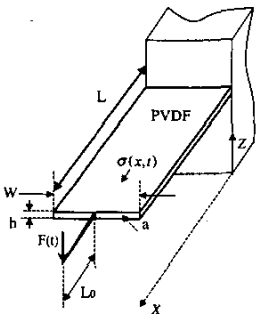

Fig. 2. 1-D force sensor

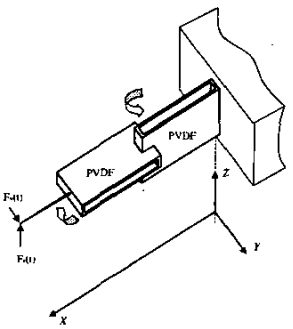

Fig. 3. 2-D force sensor

polarization factor of the PVDF film $D_3(x,t)$ can be expressed as: (without considering the inverse piezoelectric affection and pyroelectric effects)

$$D_3(x,t) = d_{31}\sigma(x,t) + \varepsilon_{33}^T E_3(t) \tag{1}$$

where d_{31} is the piezoelectrical coefficient of the PVDF film; $\sigma(x,t)$ is the unit stress; ε_{33}^T is the dielectrical factor of the PVDF film; $E_3(t)$ represents the electrical field of the PVDF film.

The total charge Q(t) across the PVDF surface area A $(L \times W)$ is

$$Q(t) = \int D_3(x,t)dA. \tag{2}$$

The unit stress on the PVDF can be calculated as

$$\sigma(x,t) = \frac{F(t)(L-x)\frac{h}{2}}{I} + \frac{F(t)L_0\frac{h}{2}}{I} \tag{3}$$

where the neutral axis of the bending deflection of beam is assumed to pass through the centroid of the cross-sectional area a. $F(t)$ is the contact force acting at the sensor tip. I denotes inertial moment of cross-sectional area a $(W \times h)$. Since the generation of charge is the same along the width of the PVDF,

$$\begin{aligned} Q(t) &= \int_0^L (d_{31}\sigma(x,t) + \varepsilon_{33}^T E_3(t))Wdx \\ &= \frac{d_{31}Ah(L_0 + \frac{L}{2})}{2I}F(t) + \varepsilon_{33}^T E_3(t)A. \end{aligned} \tag{4}$$

By the piezoelectrical effect, note that if no charge builds up by the external force, the $E_3(t)$ will be zero. Then, by an equivalent circuit model parallelling a resistor R_P and a capacitor C_P for the PVDF film. The output voltage $V(t)$ across the PVDF film, can be described by

$$\frac{V(t)}{R_P} + \dot{V}(t)C_P = \frac{dQ}{dt}. \tag{5}$$

Since the electrical field $E_3(t) = -\frac{dV(t)}{dh}$, therefore $E_3(t) = -\frac{V(t)}{h}$ for uniform electric field over the very small hight h. Thus

$$\dot{E}_3(t) = -\frac{\dot{V}(t)}{h}, \tag{6}$$

and then the relationship between the output voltage and the contact force rate can be obtained as

$$V(t) + \lambda\dot{V}(t) = B\dot{F}(t) \tag{7}$$

where $C_P = \frac{\varepsilon_{33}^T A}{h}$ is the capacitance of the PVDF film; $\lambda = 2R_P C_P$ and $B = \frac{R_P A d_{31} h(L_0 + \frac{L}{2})}{2I}$ are the constants.

By the Laplace transformation, the electrical transfer function of the PVDF sensor is given as:

$$T(s) = \frac{V(s)}{F(s)} = \frac{B}{\lambda}\frac{\lambda s}{1+\lambda s} \tag{8}$$

Based on the 1-D model, a design for 2-D PVDF force sensor has been proposed as shown in Figure 3. The 2-D sensor is designed based on a parallel beam structure. In each direction, a 2-piece parallel beam is used to improve the rigidity of the structure and, at the same time, increase the sensitivity of the force sensor in that direction. It can also be seen that this structure provides a decoupled force measurement in the Y and Z directions. The decoupled output voltages and force rates can be described as

$$\begin{aligned} V(t) + \lambda_Z\dot{V}(t) &= B_Z\dot{F}_Z(t) \\ V(t) + \lambda_Y\dot{V}(t) &= B_Y\dot{F}_Y(t) \end{aligned} \tag{9}$$

B. The Processing Circuit

Preprocessing of sensed data is critical by the circuit for two reasons: (i) remove any noise, (ii) amplify and extract the desired signal which is in this case the force. The simplified diagram of the developed circuit is shown in Figure 4.

In this circuit, a differential charge amplifier is designed for the PVDF force sensors firstly. The differential charge amplifier is based on using the chopper stabilized operational amplifier TC7650C with a high input impedance

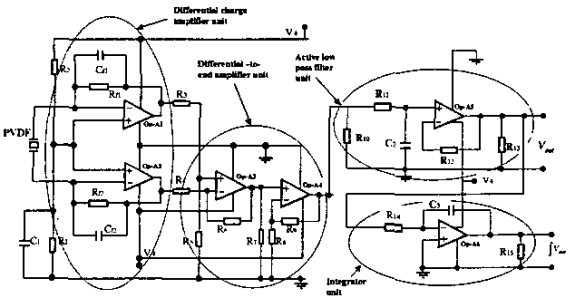

Fig. 4. Processing circuit.

$10^{12}\Omega$ and low bias current $1.5pA$. Following the charge amplifier, a differential-to-single-ended amplifier is added. The total differential topology can reduce the common mode noises more effectively. To reject the existing high frequency noises, an active low pass filter with cutoff frequency $160Hz$ is used before the voltage output. The integration of the output voltage by time can also be achieved by an integrator unit in the circuit. In addition, the reduction of RFI (Radio Frequency Interference) and EMI (Electromagnetic Interference) have been accounted for in the circuit by shielding.

C. System Transfer Function

By considering the whole circuit, the transfer function is approximated by

$$\begin{aligned} \frac{V_{out}(s)}{V(s)} &= -\frac{2R_fC_Ps}{1+R_fC_fs} \times -K_c \times \frac{1}{1+\tau_1 s} \\ &\doteq \frac{2K_cC_P}{C_f} \times \frac{1}{1+\tau_1 s} \end{aligned} \tag{10}$$

where in the circuit $R_{f1}=R_{f2}=R_f$, $C_{f1}=C_{f2}=C_f$. K_c is the gain of the differential-to-single-ended amplifier. R_f is chosen as a very large value resistor. τ_1 is a rather small time constant of the designed active low pass filter.

From eqns. (8) and (10), the global transfer function of the sensor system is

$$GT(s)=\frac{V_{out}(s)}{F(s)} \doteq \frac{K_cB}{R_PC_f}\frac{\lambda s}{(1+\lambda s)(1+\tau_1 s)}. \tag{11}$$

The function is a bandpass type filter. Since τ_1 is very small in the circuit, eqn.(11) can be rewritten as

$$GT(s)=\frac{V_{out}(s)}{F(s)} \doteq \frac{K_cB}{R_PC_f}\frac{\lambda s}{(1+\lambda s)}. \tag{12}$$

Based on this equation, the force rate and force can be generated, respectively. In a case, by integrating with respect to time, the force is obtained by measuring the output voltage of the sensor system when the initial values $F(t_0)$ and $V_{out}(t_0)$ are known.

$$F(t)-F(t_0)=\frac{C_f}{2K_cBC_P}[\lambda(V_{out}(t)-V_{out}(t_0)) + \int_{t_0}^{t} V_{out}(t)dt] \tag{13}$$

III. CONTACT FORCE CONTROL

In this section, using the force and its derivative achieved from the sensor and based on the dynamics of micromanipulator, a new sensor-referenced control method for micro contact/impact control and force regulation during microassembly is proposed. It utilizes the positive acceleration feedback together with a switching control strategy to achieve a stable micro contact/impact force regulation in microassembly.

A. Feedback Linearization

The dynamic and kinematic equations for a micromanipulator with n degrees of freedom is given by

$$\begin{cases} H(q)\ddot{q}+C(q,\dot{q})+G(q)=\tau-J^T(q)F \\ y=h(q) \end{cases} \tag{14}$$

where F is the output force in the task space, $h(q)$ represents the forward kinematics.

Upon the eqn.(14), introducing the nonlinear feedback control law:

$$\tau=H(q)J^{\#}(q)(v-\dot{J}(q)\dot{q})+C(q,\dot{q})+G(q)+J^T(q)F \tag{15}$$

where $J^{\#}(q)$ is the pseudo inverse of the Jacobian matrix. As a result, the dynamics of the micromanipulator can be linearized and decoupled as

$$\begin{aligned} \ddot{y}_u &= v_u \\ \ddot{y}_c &= v_c \end{aligned} \tag{16}$$

where y_u represents the output positions and orientation in the unconstrained directions; and y_c represents the output positions and orientation in the constrained directions. Obviously, the control in the unconstrained directions will not have an effect on dynamics in the constrained directions and vice versa.

B. Sensor-Referenced Controller

In the free motion mode, only position control is needed which can be easily implemented by proportional and derivative controller. During the phase transition and constrained motion mode, position control is used for the unconstrained directions only, i.e.,

$$v_u=\ddot{y}_u^d+k_{vu}(\dot{y}_u^d-\dot{y}_u)+k_{pu}(y_u^d-y_u), \qquad t \geq t_{sw}, \tag{17}$$

where t_{sw} represents the time of the detecting of contact/impact.

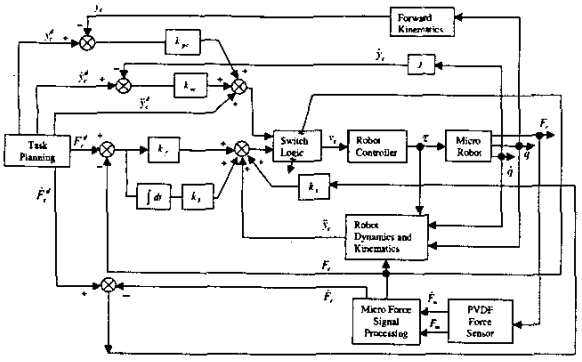

Fig. 5. Sensor-referenced control scheme for microassembly

In the constrained directions, the position control is still used before the detection of contact/impact, that is

$$v_c = \dot{y}_c^d + k_{vc}(\dot{y}_c^d - \dot{y}_c) + k_{pc}(y_c^d - y_c), \qquad t < t_{sw}. \quad (18)$$

Once the contact/impact is detected, the controller will switch from position control to force control in the constrained directions. Here, $t < t_{sw}$ is the time period of free motion mode. $t \geq t_{sw}$ is the time period of transition and constrained motion modes. Then the switching logic is given as follows.

$$\text{If } U = \{\{\dot{y}_c(t_{sw}) > 0 \cap F_c = F_{sw}\} \cup F_c < F_{sw}\}$$
$$\text{then position control}$$
$$\text{If } C = \{\{\dot{y}_c(t_{sw}) \leq 0 \cap F_c = F_{sw}\} \cup F_c > F_{sw}\}$$
$$\text{then force control} \quad (19)$$

where F_{sw} is minimum detectable force. To track the desired force during the impact mode in constrained directions, at the same time, to avoid a large impulsive force after impact, the controller is designed as:

$$v_c = \begin{cases} -k_v\dot{y}_c - k_p(y_c - y_{c,sw}) \\ \ddot{y}_c + k_s\dot{e}_f + k_f e_f + k_I \int_{t_{sw}}^{t} e_f dt. \end{cases} \quad (20)$$

The closed-loop system is:

$$\begin{cases} \ddot{y}_c + k_v\dot{y}_c + k_p(y_c - y_{c,sw}) = 0 \\ k_s\dot{e}_f + k_f e_f + k_I \int_{t_{sw}}^{t} e_f dt = 0. \end{cases} \quad (21)$$

where the position $y_{c,sw}$ corresponding to F_{sw} is unknown, but can be recorded on line to serve as the desired position for position control. $e_f = F_c^d - F_c, \dot{e}_f = \dot{F}_c^d - \dot{F}_c$. $F_c^d, F_c, k_s, k_f, k_I$ represent the desired force, the actual force response, and the force gains in the constrained directions.

The proposed contact/impact force control scheme can be illustrated by Figure 5. It is noticed that the measurement of acceleration is required, however it will be difficult to obtain a real-time acceleration measurement. Therefore, we propose to use the prior value of the acceleration calculated from the equation (14) to replace the real-time one. This method has been used in another applications with satisfactory results [8].

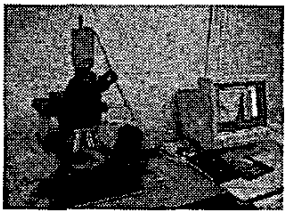

Fig. 6. A micro robotic system at MSU.

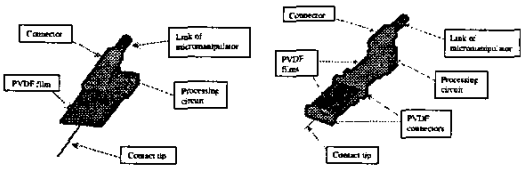

Fig. 7. Sensor's structures: (a) 1-D sensor (b) 2-D sensor

IV. EXPERIMENTS

A. Set-up

The experiments were conducted in a micro robotic system shown in Figure 6. The micro robotic system mainly consists of a SIGNATONE Computer Aided Probe Station and a Mitutoyo FS60 optical microscope system. The micro robot is controlled by a PC-based control system. The control system is an open platform which can easily integrate with the developed PVDF force sensing and control system. The PVDF force sensor (1-D) has the following dimensions and parameters: $L0 = 0.0225m; L = 0.0192m; w = 0.0102m; h = 28\mu m(PVDF film); Rp = 1.93 \times 10^{12}\Omega; Cp = 0.90 \times 10^{-9}F; E = 2 \times 10^9 N/m^2$. The sensor structures are shown in Fig. 7. The sensor system had been preliminarily calibrated with a resolution in the range of sub-μN and its sensitivity $6.0245V/\mu$N.

The force and its rate processed by the designed circuit are collected and transferred to the micro robotic system via a multifunction analog/digital input/output board AX5411H installed in a PC. There exists a communication between the PC and the micro robotic system. The sampling frequency of AX5411H is 1KHz in the experiments. The maximum encoder frequency of micromanipulator motor is 8×10^6 counts/s with 14-bit DAC resolution. The loop time of the force sensing and control system is about 2ms. To reduce the vibrations from the environment, an active vibration isolated table was used during the experiments.

B. Force Sensing

Experiments on the contact sensing will first be conducted. By using the 2-D sensor, a continual contact-stop sensing experiment is implemented when the sensor tip

acts on a planar glass surface that is set up an angle of 45 degree with respect to the ZX plane (referring to Figure 3). The 2-D force signals recorded are plotted in Fig.8. The result verifies the performance of sensing and self-decoupling of the 2-D force sensor.

C. Contact Force Control

Continually, using a 1-D sensor to contact a planar glass surface, the contact force regulation is tested. In this experiment, the path of the sensor tip consists of two segments: firstly, the sensor tip is down from a initial point in free space to a contact point on the glass surface (-Z direction), after a period of force regulation, starting from 0.76s, the sensor tip is controlled to move a straight line along Y direction on the constrained glass surface from the contact point, at the same time, the contact force is still regulated in the contact direction(Z direction). Figure 9 shows the experimental result with the setting of the desired contact force $F_c^d = 1.88 \times 10^{-6}$ Newton, the gains are $k_s = 1, k_f = 25, k_I = 25$. The results verify the performance of the developed force control scheme, that is, on the detection of the contact or in contact-motion mode, the force regulation laws make the force error go to zero asymptotically with a small peak impact force and bouncing.

D. Force-Guided Assembly of Micro Mirrors

Due to the effectiveness of the experiments on force sensing and control above mentioned, finally, a MCNC MUMPs micro mirror chip, will be used to test the developed force guided micro assembly scheme. In this experiment, the 1-D PVDF force sensor attaching a tip is mounted at the front of the 3-DOF micromanipulator. The assembly task includes multiple segments. Firstly, the tip will be moved to the position under a micro mirror. The tip, then, will lift the mirror up to an upright position until it is locked by the latches. At last, the tip will go back to the initial position and will be ready for the next assembly of micro mirror. By virtue of the developed sensor-referenced force regulation scheme, the whole assembly

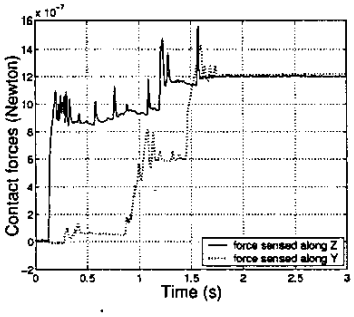

Fig. 8. 2-D sensor responses when force exerting along 45 degree with respect to the ZX plane.

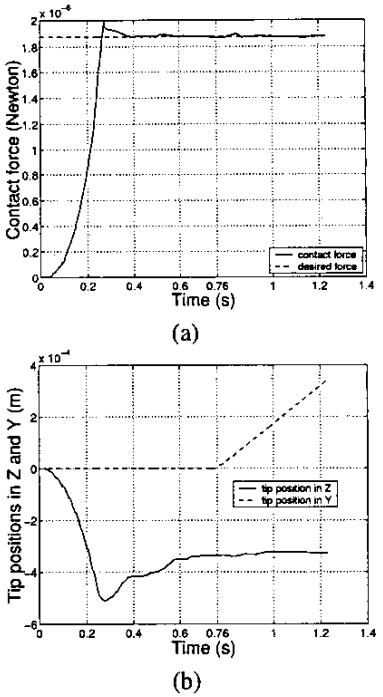

Fig. 9. Contact force control: (a) Contact force along Z (b) Tip positions in Z and Y

process can be performed automatically. The initial and final assembly statuses in Figure 10 show a successful assembly of a MCNC MUMPs micro mirror using the developed force-guided assembly scheme. Figure 11 gives a sketch of lifting up a micro mirror by the sensor tip. During the lift-up assembly, the gravity force is not a dominative force in micro environment, the forces exerted on the tip are mainly from the counteraction moments of the hinges and the latches, the friction forces when the tip sliding on the bottom surface of the mirror and the adhesion forces. Referring to Figure 11, when the tip is moved along -Y to push slowly the micro mirror up, the sensor detects the micro force and its rate along Z, the force and its rate are then fed back to the force regulation controller in real time, as a result, the contact force can be regulated to approach a desired and safe force during the lifting up. By the analysis of the action forces, to regulating the contact force along Z, the tip is adjusted automatically to slide up along the bottom surface of the micro mirror, thus it promotes the lift-up of the micro mirror until the micro mirror is locked by the latches. Force and positions data during the lift-up assembly are plotted in Figure 12 when the setting of the desired contact force is $F_c^d = 5.5 \times 10^{-7}$ Newton and the gains are $k_s = 1, k_f = 20, k_I = 20$. As shown in Figure 12(a), when the sensor tip approaches to contact the micro mirror, a downward with a spike in the force plot

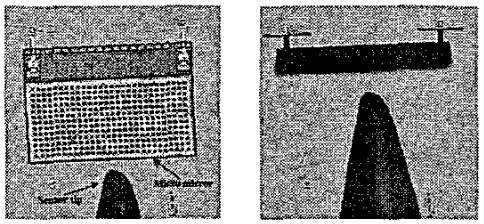

(a) (b)

Fig. 10. Micro mirror force-guided assembly: (a) a sensor tip will be moved to the position under a micro mirror (b) the automatic latches lock the mirror in upright position after lifting up by the tip using the force-guided approach.

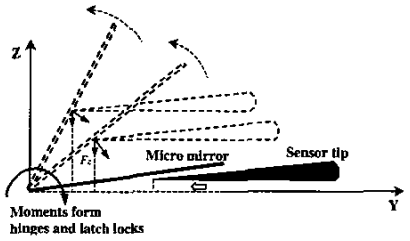

Fig. 11. Sketch of lifting up a micro mirror

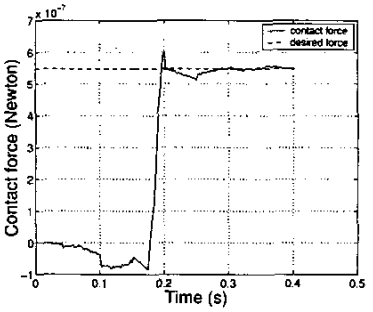

(a)

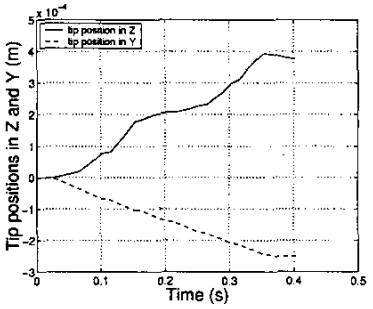

(b)

Fig. 12. 1-D Force-guided assembly results: (a) contact force along Z (b) tip positions in Y and Z.

demonstrates an adhesive force that pulls the sensor tip toward the micro mirror before the contact actually occurs. The tip positions are plotted in Figure 12(b). Experimental results verify clearly that micro mirror assembly is realized reliably by the developed force-guided assembly scheme and the micro contact force can be regulated to keep a safety margin in the assembly.

V. CONCLUSIONS

In this paper, we use polyvinylidene fluoride (PVDF) to fabricate highly sensitive force sensors for the force guided assembly of micro mirrors. By feeding back the detected force and its derivative to a new sensor-referenced controller, as a result, the micro contact force/impact can be effectively regulated so as to maintain safety margins and to greatly improve reliability during the micro mirror assembly. Experimental results verify the performance of the sensor as well as the effectiveness of the force-guided scheme. Ultimately the technology will provide a critical and major step towards the development of automated manufacturing processes for batch assembly of MEMS devices.

VI. REFERENCES

[1] J. R. Reid, V. M. Bright, J. H. Comtois. *Automated Assembly of Flip-up Micromirrors.* International Conference on Solid State Sensors and Actuators, 1997. TRANSDUCERS '97 Chicago., 1997, vol. 1. pp. 347 -350.

[2] E. E. Hui, R. T. Howe, and M. S. Rodgers. *Single-Step Assembly of Complex 3-D Microstructures.* IEEE MEMS 2000, pp. 602-607.

[3] S. K. Koelemijer Chollet, L. Benmayor, J.-M. Uehlinger and J. Jacot, *Cost Effective Micro-System Assembly Automation*, Emerging Technologies and Factory Automation. Proceedings. ETFA '99. Vol. 1, pp. 359-366, 1999.

[4] S. Fatikow, J. Seyfried, S. Fahlbusch, A. Buerkle, and F. Schmoeckel, *A Flexible Microrobot-Based Microassembly Station*, Journal of Intelligent and Robotics Systems, Vol. 27, pp. 135-169, 2000.

[5] Y. Zhou, B. J. Nelson and B. Vikramaditya. *Fusing Force and Vision Feedback for Micromanpulation* ICRA1998, pp. 1220-1225, 1998.

[6] T. Tanikawa, M. Kawai, N. Koyachi, T. Arai, T. Ide, S. Kaneko, R. Ohta and T. Hirose. *Force Control System for Autonomous Micro Manipulation*, ICRA2001, pp. 610-615, 2001.

[7] C. K. M. Fung, I. Elhajj, W. J. Li, and N. Xi *A 2-D PVDF Force Sensing System for Micro-manipulation and Micro-assembly*, ICRA2002, pp. 1489-1494, 2002

[8] T. J. Tarn, Y. Y. Wu, N. Xi, and A. Isidori, *Force Regulation and Contact Transition Control*, IEEE Control Systems, pp. 32-40, February 1996.